Plasmonic Metasurface "Bullets" and other "Moving Objects": Spatiotemporal Dispersion Cancellation for Linear Passive Subwavelength Slow Light

Aristeidis Karalis[1,*] and J. D. Joannopoulos[1,2]
[1]Research Laboratory of Electronics, Massachusetts Institute of Technology, Cambridge, Massachusetts 02139, USA
[2]Department of Physics, Massachusetts Institute of Technology, Cambridge, Massachusetts 02139, USA

(Received 12 December 2018; published 8 August 2019)

A class of plasmonic metasurfaces is introduced with the ability to tailor the dispersion surface of the associated plasmon-polariton into striking novel shapes. Examples include dispersion surfaces with hyperbolic curves, with multiple van Hove singularities of various types or with points of simultaneous spatiotemporal dispersion cancellation leading to unprecedented surface flatness. The latter effect, unseen before in linear passive systems, implies slow propagation of ultrasubwavelength wave packets of any shape devoid of longitudinal or lateral broadening, limited only by absorption.

DOI: 10.1103/PhysRevLett.123.067403

In the perennial effort to mold the flow of light at will, one fundamental issue has always stood as an obstacle: dispersion, the tendency of light wave packets to spread out as they propagate. It appears in many types, according to the dimensionality of the propagation. In one dimension x, such as a straight waveguide, curvature in the dependence $k_x(\omega)$ of wave vector on frequency is called temporal dispersion or, equivalently seen as $\omega(k_x)$, spatial-longitudinal dispersion (pulse broadening in the direction of propagation). Scientists have devised methods to *compensate* temporal dispersion, including via nonlinearities leading to temporal solitons [1], or waveguide designs to actually *cancel* (namely, *eliminate*) it to high orders [2,3]. For propagation along x in a two-dimensional (2D) system xy, a constant-frequency narrow beam will diverge or diffract, if the dependence $k_x(k_y)$ of longitudinal on transverse wave vector has curvature, or, seen as curvature in $\omega(k_y)$, a pulsed beam infinite in x will disperse spatially transversely (in y). Diffraction has been countered either again via nonlinear *compensation* and spatial soliton beam formation [1,4] or via *cancellation* in flat equifrequency dispersion curves (EFDC), named supercollimation, of 2D photonic crystals [5,6] and of hyperbolic plasmonic metasurfaces [7,8]. For pulse propagation in two dimensions, both temporal (spatial-longitudinal) and spatial-transverse dispersions occur, and only *nonlinear* spatiotemporal solitons [1,4,9–11] and linear wave packets of preprepared *specific shapes* (Airy-Bessel) [12] have been shown to form "light bullets" by *balancing* both types. They have never been simultaneously canceled before. In this Letter, we present a *linear* passive plasmonic metasurface platform, which accomplishes simultaneous spatiotemporal dispersion cancellation (STDC) for subwavelength slow surface plasmon polariton (SPP) modes [13], leading to propagation without broadening for ultrashort 2D pulses, namely plasmonic "bullets," and generally for subwavelength 2D wave packets of *any shape*, akin to "moving objects." We emphasize that these effects relate to in-plane metasurface propagation, in contrast to plasmonic metasurfaces involving transmissive functionality [14,15].

Tuning the photonic density of states (PDOS) of a structure is fundamental for controlling or enhancing light-matter interactions. Systems with hyperbolic dispersion [16–18] exhibit theoretically divergent PDOS, so are promising for boosting spontaneous or thermal emission and could have applications in imaging. In a 2D dispersion surface, van Hove extrema-type singularities [19] lead to steps in the PDOS and saddle-type points, previously encountered only in 2D photonic crystals [20,21], to logarithmic PDOS divergences, both PDOS features extremely useful for high-frequency-sensitivity sensors and filters. Our currently proposed SPP platform can be tuned to also give a variety of exotic dispersion surfaces, including hyperbolic behavior, extrema- or saddle-type van Hove singularities, or all of these simultaneously.

Consider a SPP propagating along x on a metallic surface defining the xy plane with dielectrics above it ($z > 0$). For a common isotropic planar system with continuous xy-translational and z-rotational symmetries, the EFDC $\omega(k_x, k_y)$ are circles, with ω dependent only on $\sqrt{k_x^2 + k_y^2}$, so $D^x_{y^2} \equiv k_x \partial^2 k_x / \partial k_y^2|_{k_y=0}$, the leading dispersion coefficient causing diffraction, is $D^x_{y^2} = -1$. In order to instead achieve supercollimation ($D^x_{y^2} = 0$), the rotational symmetry needs to be broken. The standard way is to use 2D periodicity in the xy plane [5,6], but here we begin by considering a uniform system with anisotropy. Let the space $z > 0$ be occupied by a uniform uniaxial dielectric with its optical axis along x [inset of Fig. 1(a)]. This system has been analyzed [7,22] and shown to exhibit

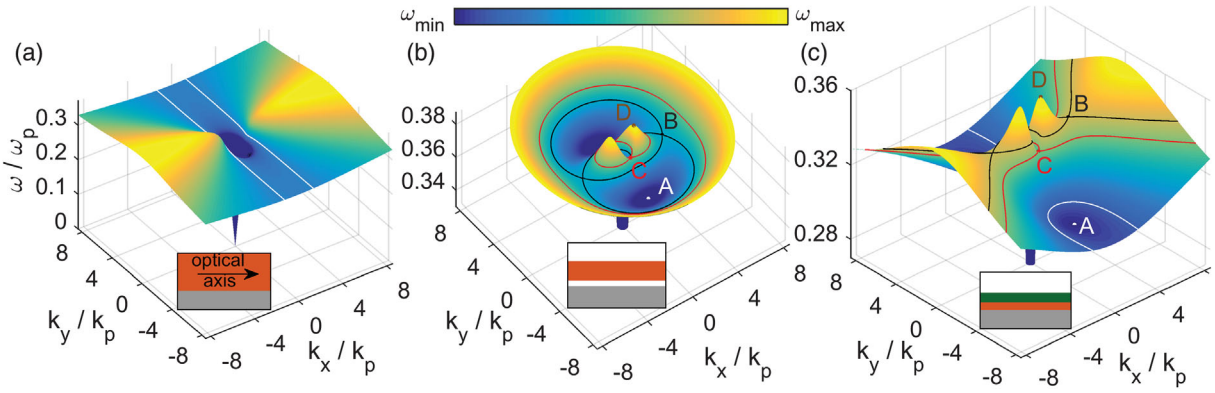

FIG. 1. $\omega(k_x, k_y)$ dispersion diagrams for the planar z-layered SPP systems in insets, with silver (gray) and dielectrics on top of it: (a) semi-infinite uniaxial (red) ($\varepsilon_{o,yz} = 6.45$, $\varepsilon_{e,x} = 1.845$), (b) air($d = 0.005\lambda_p$)-uniaxial (red) ($\varepsilon_{o,yz} = 8.1$, $\varepsilon_{e,x} = 6.317$, $d = 0.032\lambda_p$)-air, (c) uniaxial (red) ($\varepsilon_{o,yz} = 6.45$, $\varepsilon_{e,x} = 1.845$, $d = 0.035\lambda_p$)-isotropic (green) ($\varepsilon = 11.9$, $d = 0.023\lambda_p$)-air. [TDOS vs frequency for (b) is shown in the Supplemental Material [28], Fig. S1.] (a),(c) White lines are EFDC, above which hyperbolic dispersion starts (and thus TDOS diverges). (b),(c) Black and red lines are EFDC passing through saddle-type van Hove points B,C, respectively. Points A are minima and D maxima.

hyperbolic dispersion within some frequency range. The dispersion for $\varepsilon_o = 6.45$, $\varepsilon_e = 1.845$ is shown in Fig. 1(a), where, at low frequencies, EFDC are ellipses, so $D^x_{y^2} < 0$, while, at higher frequencies, EFDC indeed become hyperbolas, so $D^x_{y^2} > 0$; therefore, there is a frequency where supercollimation $D^x_{y^2} = 0$ occurs (true for any 2D hyperbolic system [7,8]). For definiteness, in all results presented in this Letter, the metal is silver (Ag) and was modeled by a Drude permittivity with $\varepsilon_\infty = 4$, plasma frequency $\omega_p = 9.3\ \mathrm{eV}/\hbar = ck_p = 2\pi c/\lambda_p$, and $\gamma/\omega_p = 0.0025$ intrinsic bulk losses at room temperature [23–26], but nonlocal Landau surface damping [27] was ignored to avoid complexity.

References [3,29] motivated using ultrathin dielectric layers with alternating high and low index on top of the metal to create interesting z-rotationally invariant SPP dispersion relations, including the cancellation of temporal dispersion to high orders. The underlying principle was that, at small k, the SPP field extends far from the metallic interface and thus "sees" more of the outermost dielectric layer, while, as k increases, the field is more tightly bound to the interface, so is affected more by the innermost layers. The same idea holds when we include uniaxial layers. Figures 1(b), 1(c) show the dispersion for two such systems. Their qualitative difference is that, at large k, they asymptote to circular and hyperbolic dispersions, respectively, because the closest layer to the metal is correspondingly air and a uniaxial dielectric. More importantly however, in both cases, very interesting and unusual features are present, specifically several van Hove singularities [19]: two minima A, two sharp maxima D, and four saddle points B,C. For Fig. 1(b), their associated impacts in the total density of states (TDOS) are, as expected, a large positive step at minimum A, log peaks at saddles B,C and a small negative step at maximum D, as shown in Fig. S1 of the Supplemental Material, Sec. B [28], where we describe also the TDOS calculation details [30–32]. Such singularities have so far only been associated with 2D-periodic systems [20,21], but here we show that they are, perhaps counterintuitively, possible also for xy-translationally invariant systems, which combine the special properties of SPPs with anisotropicity. The calculations for multilayered structures including uniaxial dielectric media (in Figs. 1, 2) were done using a scattering-matrix method [33,34] based on the formulation in Ref. [35], as presented in detail in the Supplemental Material, Sec. A [28].

Furthermore, since a planar distribution of ultrathin isotropic layers can lead to temporal (or spatial-longitudinal) dispersion cancellation [3] and uniaxial layers can result in supercollimation (spatial-transverse dispersion cancellation), our main goal is to examine if the presently proposed combination of isotropic and uniaxial dielectric layers can lead to a SPP with simultaneous (longitudinal and transverse) STDC. Considering all optical axes of uniaxial layers to lie in the x direction, then $\omega(k_x, -k_y) = \omega(k_x, k_y)$. Therefore, if $D_{n,m} \equiv \omega_0^{n-1}\partial^{n+m}\omega/\partial k_x^n \partial k_y^m|_{k_{x0},0}$ are the normalized dimensionless dispersion constants of the (n,m)th order at the point $(k_{x0}, 0, \omega_0)$, then $D_{n,m} = 0$ for m odd and $v_{g0} \equiv cD_{1,0}$ is the group velocity along x ($D_{0,1} = 0$). STDC would mean that we can design a system with $D_{2,0} = D_{0,2} = 0$ (note $D_{1,1} = 0$ anyway). Even better then, in Fig. 2 we present results for a structure that supports a SPP mode with $D_{2,0} = D_{0,2} = D_{3,0} = 0$, namely, the first nonzero dispersion terms are $D_{1,2}$, $D_{4,0}$, $D_{2,2}$, and $D_{0,4}$, which are high-order terms with small impact to pulse propagation, as we will see. Although several configurations within our proposed system can achieve this cancellation, the simplest structure presented here [shown in the inset of Fig. 2(a)] entails placing on the metal interface only a very thin dielectric ($\varepsilon = 11.9$) layer and an even thinner uniaxial layer ($\varepsilon_o = 6.45$, $\varepsilon_e = 1.845$).

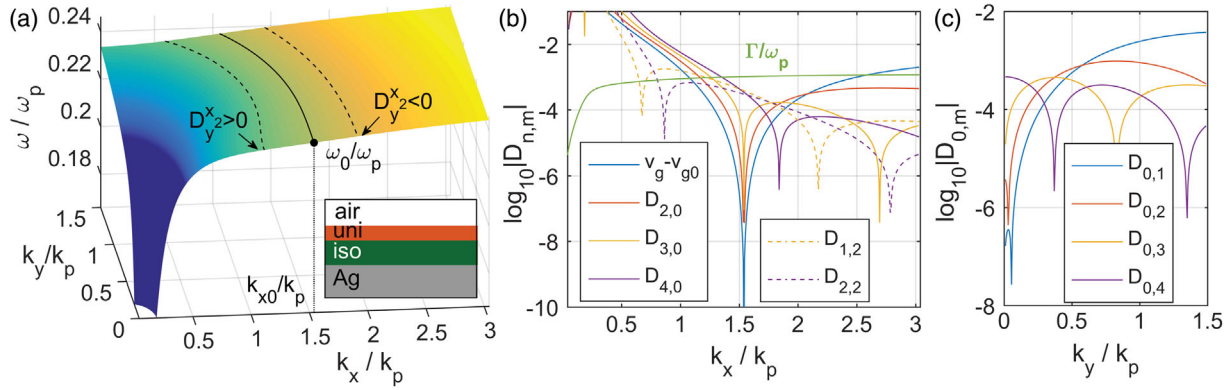

FIG. 2. (a) $\omega(k_x, k_y)$ for the inset z-layered SPP system with Ag, iso($\varepsilon = 11.9$, $d = 0.138\lambda_p$), uni($\varepsilon_{o,yz} = 6.45$, $\varepsilon_{e,x} = 1.845$, $d = 0.0483\lambda_p$): note the extremely flat regime around ($k_{x0}/k_p = 1.540$, $k_{y0} = 0$, $\omega_0/\omega_p = 0.237 - 0.00103i$) with $v_{g0}/c = 0.0053$; 3 EFDC demonstrate supercollimation at the cancellation point. (b) (all lines except green) $D_{n,m}$ dispersion coefficients [namely, derivatives of (a)] along k_x: $D_{2,0} = D_{3,0} = 0$ = canceled at $(k_{x0}, 0)$. (green line) $\Gamma = -\mathrm{Im}(\omega)$ loss rate: note that, as $k_x \to \infty$, $\Gamma \to \gamma/2$ intrinsic limit [3,36]. (c) $D_{0,m}$ coefficients [k_y derivatives of (a)] along k_y: again $D_{0,1} = D_{0,2} = D_{0,3} = 0$.

The dispersion surface shown in Fig. 2(a) around the cancellation point is the flattest plane ever demonstrated, to our knowledge, for a linear passive photonic structure. Note that, since $D^x_{y^2} = k_x(\partial^2 k_x/\partial k_y^2) = k_x(\partial/\partial k_y)[-(\partial\omega/\partial k_y)/(\partial\omega/\partial k_x)] = k_x[-(\partial^2\omega/\partial k_y^2)v_{g0} + (\partial\omega/\partial k_y)(\partial^2\omega/\partial k_x\partial k_y)]/v_{g0}^2 = -k_x D_{0,2}/\omega_0 v_{g0} = 0$, supercollimation is achieved also in the traditional sense, as indicated with the EFDC shown in Fig. 2(a).

Unfortunately, in practice, there are no materials with such large anisotropy. Nevertheless, we can create an effective uniaxial metamaterial with $\varepsilon_o = (\varepsilon_1 + \varepsilon_2)/2$ and $\varepsilon_e^{-1} = (\varepsilon_1^{-1} + \varepsilon_2^{-1})/2$, by layering two dielectrics with permittivities ε_1, ε_2 and the same thickness along the desired optical axis with a period smaller than the propagation wavelength $\lambda_{x0} = 2\pi/k_{x0}$ [Fig. 3(a)] [7,37]. To get $\varepsilon_o = 6.45$, $\varepsilon_e = 1.845$, we have to use $\varepsilon_1 = 1$ (air) and $\varepsilon_2 = 11.9$, which is the permittivity of GaP at the frequency $\hbar\omega_0 \approx 0.237 \times 9.3$ eV $= 2.2$ eV, where GaP is also transparent (see Supplemental Material, Sec. C [28]). As shown in Fig. 3(b), slicing a thin z layer of this metamaterial creates simply a grating on top of the uniform GaP layer. Using an analytical model for the material dispersion of GaP [see Supplemental Material [28], Fig. S2(a)] [38], the Bloch modes of this grating metasurface were calculated with COMSOL [39]. Our desired STDC ($D_{2,0} = D_{0,2} = D_{3,0} = 0$) is achieved also for this periodic structure, for period $a = 0.236\lambda_{x0}$ and optimized parameters close to those of the xy-uniform system with nondispersive dielectric materials. This justifies the effective metamaterial design approach and shows that dielectric material dispersion, although included here for accuracy, is a much weaker effect than the geometric dispersion control imposed by our mechanism in plasmonics. The periodic part of the modal magnetic field $\mathbf{H}$ at $(k_{x0}, 0, \omega_0)$ is shown in Fig. 3(c), and the $\omega(k_x, k_y)$ dispersion in Fig. 3(d) is superflat and almost identical to Fig. 2(a). With $\lambda_0 = cT_0 = 2\pi c/\omega_0$ the free-space wavelength, this

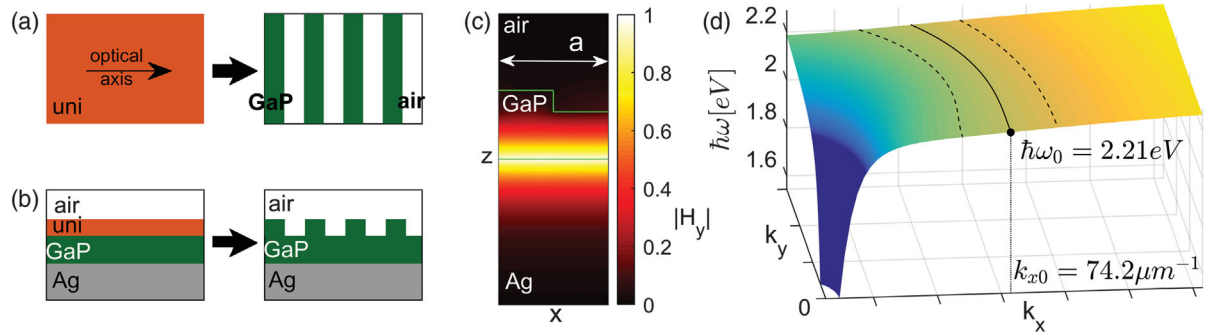

FIG. 3. (a) A uniaxial dielectric with optical axis along x (left) created effectively via x-periodic layering of two isotropic dielectrics (GaP-air) with same thickness (right). (b) The structure of Fig. 2 (left) emulated via z slicing the effective uniaxial of (a) into a GaP grating metasurface (right). (c) Periodic part of the Bloch mode $F(k_{x0}, k_{y0}; x, z)$ for the SPP metasurface in (b-right) with $d_{\mathrm{film}} = 0.13\lambda_p = 17.3$ nm, $d_{\mathrm{grating}} = 0.059\lambda_p = 7.9$ nm, and $a = 0.15\lambda_p = 20$ nm, at ($k_{x0}/k_p = 1.576$, $k_{y0} = 0$, $\omega_0/\omega_p = 0.238 - 0.00104i$) and with $v_{g0}/c = 0.004$. (d) $\omega(k_x, k_y)$ dispersion surface: exactly same qualitative features as Fig. 2.

unique SPP STDC is accomplished for a very subwavelength mode, truly plasmonic longitudinally ($\lambda_{x0} n_{\mathrm{GaP}}/\lambda_0 = 0.52$) and vertically ($d_z^{\mathrm{eff}} 4 n_{\mathrm{GaP}}/\lambda_0 = 0.28$, where $d_z^{\mathrm{eff}} a = \iint \mu_0 |\mathbf{H}|^2 dx dz / \max\{\mu_0 |\mathbf{H}|^2\}$), for very slow light at $v_{g0} = 0.004c$, and with quality factor due to the metal absorption $Q = \omega_0/2\Gamma_0 = 115$.

To understand the benefits of STDC in wave packet propagation, we compare the evolution of a pulse centered at $(k_{x0}, 0, \omega_0)$ for our metasurface of Fig. 3 to a classic SPP on the interface between silver and an isotropic dielectric of $\varepsilon = 10.405$, such that this SPP crosses $(k_{x0}, 0, \omega_0)$, with similar $Q = 118$, but larger $v_{g0} = 0.0293c$ and nonzero $D_{2,0} = -0.0115$, $D_{0,2} = 0.00443$ (note $D^{x}_{y^2} = -k_{x0} D_{0,2}/\omega_0 v_{g0} = -1$ is confirmed). Specifically, we consider an initial Gaussian pulse envelope $|\mathbf{H}(x, y, t = 0)|^2 = \exp(-x^2/2\sigma_{x0}^2 - y^2/2\sigma_{y0}^2)$ with ultrashort widths $\sigma_{x0} = \sigma_{y0} = \lambda_0/20 = 28$ nm, and this green-light ($\lambda_0 = 560$ nm) pulse is shown in Fig. 4(a). Then we calculate numerically (details in Supplemental Material, Sec. E [28]), at any time t, the field, whose intensity is reduced due to both absorption and dispersion. In Figs. 4(b), 4(c), it is shown for the classic SPP and our metasurface at $t = 36T_0$, chosen to correspond to a reduction of peak intensity to 10% for the latter. Impressively, this pulse maintains its shape for much longer, basically until extinguished by absorption (as shown in Supplemental Material [28], video for $t \leq 100T_0$), and can be thought of as a "plasmonic bullet." In contrast, the classic-SPP system has led to significant broadening, both longitudinally and transversely, and much worse intensity reduction. The pulse widths σ_{xt}, σ_{yt} and peak intensity I_{ot} are calculated numerically [shown in Supplemental Material [28], Fig. S2(b) for $t \leq 100T_0$] and fit, respectively, to an approximate time dependence $\sqrt{[\sigma_{xt}, \sigma_{yt}]^2 - \sigma_0^2}/\lambda_0 \approx [0.024, 0.013]\tau$, $I_{ot} \exp(2\pi\tau/Q) \approx 1/(1 + 0.12\tau + 0.014\tau^2 + 0.00013\tau^3)$, $\tau \equiv t/T_0$ for the classic SPP and $\approx [0.0064, 0.0040]\tau$, $\approx 1/(1 + 0.0085\tau + 3.7 \times 10^{-5}\tau^2)$ for the metasurface. The latter broadening is 3.7 times smaller and would be substantially smaller for broader initial pulses (in the Supplemental Material, Sec. E [28], we calculate σ_{xt}, σ_{yt} also analytically, using a procedure similar to Ref. [40]). For the simple SPP, absorption decay $\exp(-2\pi\tau/Q)$ is weaker than dispersion decay for $t < 110T_0$ [e.g., at $t = 36T_0$ in Fig. 4(b), 0.147 vs $0.005/0.147 = 0.034$, respectively]. Therefore, despite the notorious losses in plasmonics, dispersion can surprisingly be a much more detrimental effect than absorption, for short enough pulses. STDC can thus maintain large localized field intensities for longer time, which could be useful to prolong interactions of plasmonic bullets with comoving nanoparticles and for dynamic nanosensors.

The main advantage of *linear* STDC is that dispersionless propagation is pulse-shape independent. In Figs. 4(d)–4(f), an initial green-light packet arbitrarily shaped to spell "MiT" with subwavelength features is let propagate through the two compared structures. It is utterly unrecognizable at $t = 36T_0$ on the isotropic SPP, but an almost-intact-shape "moving object" on our STDC Ag/GaP meta-surface SPP, just attenuated from the silver

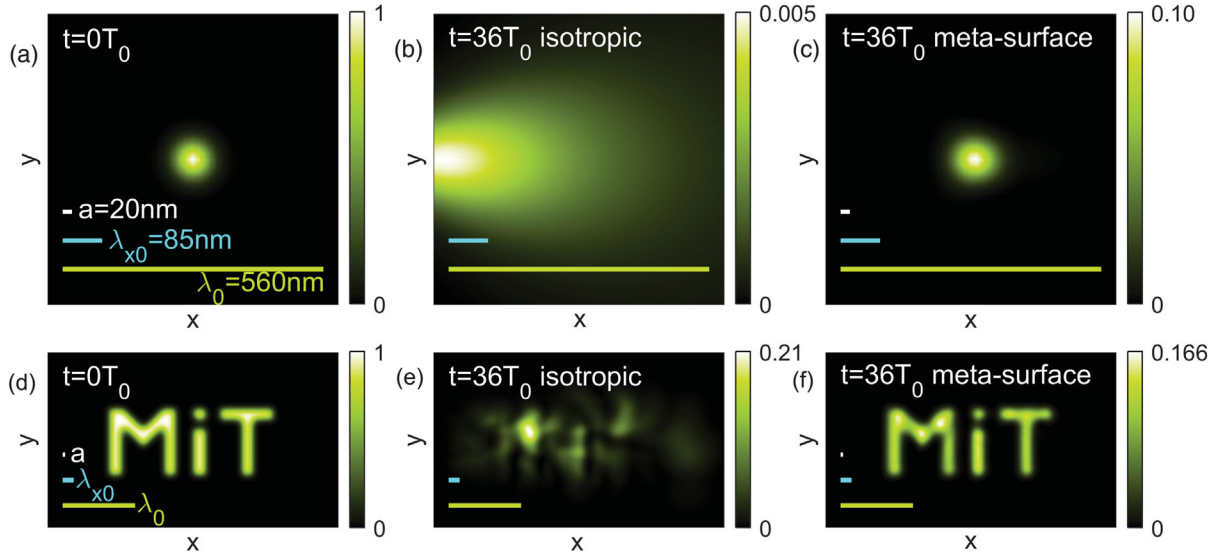

FIG. 4. Propagating wave packet field intensities $|H(x, y, t)|^2$ centered around $x = v_{g0}t$ for initial ultrashort wave packets: (a)–(c) a Gaussian pulse and (d)–(f) a packet spelling MiT; the color bar is scaled on each plot to show the peak intensity. (a),(d) Wave packet at $t = 0$ (initial), (b),(e) at $t = 36T_0$ for classic isotropic SPP, whose dispersion crosses the same $(k_{x0}, 0, \omega_0)$ point, and (c),(f) for the metasurface of Fig. 3. In (e), peak intensity is relatively large due to superposition in one location of different parts of the heavily dispersed wave packet.

absorption. The regime around supercollimation in hyperbolic materials has been termed "hyperlens" and its relation to subwavelength imaging over short ranges discussed [7,41,42]. With our added temporal dispersion cancellation, one could now extend this discussion to real-time subdiffraction short-range video imaging.

The unavoidable metal absorption loss is the major practical drawback of plasmonics. At least, since our proposed platform uses only one flat unpatterned metallic surface, it maintains the advantage of the lower expected losses associated with dielectric-loaded-SPPs [29] by avoiding boundary electronic scattering [26], present in common plasmonic metasurfaces involving patterning of the metal. Furthermore, in the Supplemental Material, Sec. D [28] we show the spectacular result that, if we used a semiconductor ($Ga_xIn_{1-x}P$) [43] with direct band gap slightly lower than the STDC frequency and if we could achieve the necessary population inversion [44,45] (difficult via current injection for such subwavelength systems [46], but possible with optical pumping), the net modal loss-gain rate $\Gamma(k_x, k_y) = -\mathrm{Im}[\omega(k_x, k_y)]$ could be designed to still always be positive, thus preventing "spasing" at any frequency and ensuring stable propagation, but minimum and zero at the STDC point to achieve full loss compensation ($\Gamma_0 = 0$) with simultaneous loss-dispersion cancellation ($\partial\Gamma_0/\partial k_x = 0$) (and hence slightly reducing too the huge spontaneous emission [47]). This would signify true unprecedented "moving light-objects."

Different metal/semiconductor combinations can also be used for operation at other visible frequencies, for example, Ag/AlN for violet (~400 nm), Ag/ZnS for blue (~440 nm), and Au/GaP for red (~660 nm), and lower frequencies could be reached by making the metal a thin film [13]. Just as in Ref. [3], by including additional layers, higher-order cancellations are possible, but there are limits to k_{x0}, v_{g0}, for which they can be attained. Moreover, we confirmed our proposed effective transformation works not only for dispersion cancellation but also for the exotic dispersions in Fig. 1.

This work was supported in part by the U.S. Army Research Office through the MIT Institute for Soldier Nanotechnologies under Contract No. W911NF-13-D-0001. (2282)

*aristos@mit.edu

[1] Y. S. Kivshar and G. P. Agrawal, *Optical Solitons: From Fibers to Photonic Crystals* (Academic Press, London, 2003).
[2] J. B. Khurgin, Opt. Lett. **30**, 513 (2005).
[3] A. Karalis, J. D. Joannopoulos, and M. Soljačić, Phys. Rev. Lett. **103**, 043906 (2009).
[4] Z. Chen, M. Segev, and D. N. Christodoulides, Rep. Prog. Phys. **75**, 086401 (2012).
[5] H. Kosaka, T. Kawashima, A. Tomita, M. Notomi, T. Tamamura, T. Sato, and S. Kawakami, Appl. Phys. Lett. **74**, 1212 (1999).
[6] P. T. Rakich, M. S. Dahlem, S. Tandon, M. Ibanescu, M. Soljačić, G. S. Petrich, J. D. Joannopoulos, L. A. Kolodziejski, and E. P. Ippen, Nature (London) **5**, 93 (2006).
[7] Z. Jacob and E. E. Narimanov, Appl. Phys. Lett. **93**, 221109 (2008).
[8] Y. Yang, L. Jing, L. Shen, Z. Wang, B. Zheng, H. Wang, E. Li, N.-H. Shen, T. Koschny, C. M. Soukoulis *et al.*, Asia Mater. **9**, e428 (2017).
[9] B. A. Malomed, D. Mihalache, F. Wise, and L. Torner, J. Opt. B **7**, R53 (2005).
[10] S. Minardi, F. Eilenberger, Y. V. Kartashov, A. Szameit, U. Röpke, J. Kobelke, K. Schuster, H. Bartelt, S. Nolte, L. Torner *et al.*, Phys. Rev. Lett. **105**, 263901 (2010).
[11] D. Majus, G. Tamošauskas, I. Gražulevičiūtė, N. Garejev, A. Lotti, A. Couairon, D. Faccio, and A. Dubietis, Phys. Rev. Lett. **112**, 193901 (2014).
[12] A. Chong, W. H. Renninger, D. N. Christodoulides, and F. W. Wise, Nat. Photonics **4**, 103 (2010).
[13] S. A. Maier, *Plasmonics: Fundamentals and Applications* (Springer, New York, NY, 2007).
[14] N. Yu and F. Capasso, Nat. Mater. **13**, 139 (2014).
[15] A. V. Kildishev, A. Boltasseva, and V. M. Shalaev, Science **339**, 1232009 (2013).
[16] A. Poddubny, I. Iorsh, P. Belov, and Y. Kivshar, Nat. Photonics **7**, 958 (2013).
[17] L. Ferrari, C. Wu, D. Lepage, X. Zhang, and Z. Liu, Prog. Quantum Electron. **40**, 1 (2015).
[18] I. I. Smolyaninov and V. N. Smolyaninova, Solid-State Electron. **136**, 102 (2017).
[19] L. van Hove, Phys. Rev. **89**, 1189 (1953).
[20] M. Ibanescu, E. J. Reed, and J. D. Joannopoulos, Phys. Rev. Lett. **96**, 033904 (2006).
[21] X. Lin, X. Zhang, L. Chen, M. Soljačić, and X. Jiang, Opt. Express **21**, 30140 (2013).
[22] R. Li, C. Cheng, F.-F. Ren, J. Chen, Y.-X. Fan, J. Ding, and H.-T. Wang, Appl. Phys. Lett. **92**, 141115 (2008).
[23] P. B. Johnson and R. W. Christy, Phys. Rev. B **6**, 4370 (1972).
[24] S. Babar and J. H. Weaver, Appl. Opt. **54**, 477 (2015).
[25] Y. Wu, C. Zhang, M. N. Estakhri, Y. Zhao, J. Kim, M. Zhang, X.-X. Liu, G. K. Pribil, A. Alú, C.-K. Shih *et al.*, Adv. Mater. **26**, 6106 (2014).
[26] W. Chen, K. P. Chen, M. D. Thoreson, A. V. Kildishev, and V. M. Shalaev, Appl. Phys. Lett. **97**, 211107 (2010).
[27] J. B. Khurgin, Faraday Discuss. **178**, 109 (2015).
[28] See Supplemental Material at http://link.aps.org/supplemental/10.1103/PhysRevLett.123.067403 for informational text Sections A–E and two comparative videos of wave packet propagation.
[29] A. Karalis, E. Lidorikis, M. Ibanescu, J. D. Joannopoulos, and M. Soljačić, Phys. Rev. Lett. **95**, 063901 (2005).
[30] A. J. Morris, R. J. Nicholls, C. J. Pickard, and J. R. Yates, Comput. Phys. Commun. **185**, 1477 (2014).
[31] K. Busch and S. John, Phys. Rev. E **58**, 3896 (1998).
[32] B. Liu, S. G. Johnson, J. D. Joannopoulos, and L. Lu, J. Opt. **20**, 044005 (2018).
[33] P. Bienstman and R. Baets, Opt. Quantum Electron. **33**, 327 (2001).

[34] P. Bienstman and R. Baets, Opt. Quantum Electron. **34**, 523 (2002).
[35] P. Yeh, Surf. Sci. **96**, 41 (1980).
[36] J. B. Khurgin and A. Boltasseva, MRS Bull. **37**, 768 (2012).
[37] V. M. Agranovich and V. E. Kravtsov, Solid State Commun. **55**, 85 (1985).
[38] S. Adachi, J. Appl. Phys. **66**, 6030 (1989).
[39] COMSOL MULTIPHYSICS® v. 5.1, www.comsol.com, COMSOL AB, Stockholm, Sweden.
[40] G. P. Agrawal, *Nonlinear Fiber Optics*, 3rd ed. (Academic Press, San Diego, CA, 2001).
[41] Z. Liu, H. Lee, Y. Xiong, C. Sun, and X. Zhang, Science **315**, 1686 (2007).
[42] I. I. Smolyaninov, Y.-J. Hung, and C. C. Davis, Science **315**, 1699 (2007).
[43] Y. A. Goldberg, in *Handbook Series on Semiconductor Parameters*, Vol. 2, edited by M. Levinshtein, S. Rumyantsev, and M. Shur (World Scientific, Singapore, 1996), Chap. 2, pp. 37–61.
[44] S. Balle, Phys. Rev. A **57**, 1304 (1998).
[45] A. Cerjan, Y. D. Chong, and A. D. Stone, Opt. Express **23**, 6455 (2015).
[46] J. B. Khurgin and G. Sun, Appl. Phys. Lett. **100**, 011105 (2012).
[47] A. A. Vyshnevyy and D. Y. Fedyanin, Phys. Rev. Applied **6**, 064024 (2016).